



**HAL**  
open science

## On the accuracy limits of plate theories for vibro-acoustic predictions

U. Arasan, F. Marchetti, F. Chevillotte, G. Tanner, D. Chronopoulos, E.  
Gourdon

► **To cite this version:**

U. Arasan, F. Marchetti, F. Chevillotte, G. Tanner, D. Chronopoulos, et al.. On the accuracy limits of plate theories for vibro-acoustic predictions. *Journal of Sound and Vibration*, 2021, 493, pp.115848. 10.1016/j.jsv.2020.115848 . hal-03493243

**HAL Id: hal-03493243**

**<https://hal.science/hal-03493243>**

Submitted on 15 Dec 2022

**HAL** is a multi-disciplinary open access archive for the deposit and dissemination of scientific research documents, whether they are published or not. The documents may come from teaching and research institutions in France or abroad, or from public or private research centers.

L'archive ouverte pluridisciplinaire **HAL**, est destinée au dépôt et à la diffusion de documents scientifiques de niveau recherche, publiés ou non, émanant des établissements d'enseignement et de recherche français ou étrangers, des laboratoires publics ou privés.



Distributed under a Creative Commons Attribution - NonCommercial 4.0 International License

1                    On the accuracy limits of plate theories for  
2                    vibro-acoustic predictions

3                    U. Arasan<sup>a,b,c,\*</sup>, F. Marchetti<sup>a</sup>, F. Chevillotte<sup>a,\*</sup>, G. Tanner<sup>b</sup>, D.  
4                    Chronopoulos<sup>c</sup>, E. Gourdon<sup>d</sup>

5                    <sup>a</sup>*Matelys - Research Lab, F-69120 Vaulx-en-Velin, France*

6                    <sup>b</sup>*School of Mathematical Sciences, University of Nottingham, University Park, NG7*  
7                    *2RD, UK*

8                    <sup>c</sup>*Institute for Aerospace Technology and The Composites Group, University of*  
9                    *Nottingham, University Park, NG7 2RD, UK*

10                    <sup>d</sup>*Université de Lyon, ENTPE, LTDS UMR CNRS 5513, 3 rue Maurice Audin, 69518*  
11                    *Vaulx-en-Velin Cedex, France*

---

12    **Abstract**

Several vibro-acoustic models for either single wall or multi-layer constructions are based on classical plate and first order shear deformation theories. The equivalent or condensed plate models employ the thin plate model to extract the dynamic mechanical properties of the multi-layer system considering only flexural and shear motions for the structure under investigation. Since these plate models do not account for the compressional or symmetric motion of the structure, both thin and thick plate theories encounter limitations for mid to high frequency predictions depending on the structures considered. In this work, analytical expressions for the frequency limit of thin and thick plate theories are derived for an elastic layer of isotropic material from the analyses of wavenumbers and admittances. Additionally, refined expressions for coincidence and critical frequencies are presented. Validation of these frequency limits are made by comparing the transmission loss (TL) obtained from both plate theories with the TL computed through the theory of elasticity for a range of thin/thick and soft/stiff materials.

13    *Keywords:* Wavenumbers, Thin plate theory, Thick plate theory, Elasticity  
14    theory, Coincidence frequency, Critical frequency

---

\*Corresponding authors:

*Email addresses:* [arasan.uthaysuriyan@matelys.com](mailto:arasan.uthaysuriyan@matelys.com) (U. Arasan),  
[fabien.chevillotte@matelys.com](mailto:fabien.chevillotte@matelys.com) (F. Chevillotte)

*Preprint submitted to Elsevier*

*October 29, 2020*

15 **NOMENCLATURE**

$h$	Thickness	$\theta$	Incident angle
$k_0$	Wavenumber in the air	$k_t$	Transverse wavenumber
$k_p$	Natural propagating wavenumber	$k_b$	Bending wavenumber
$k_s$	Corrected shear wavenumber	$k_m$	Membrane wavenumber
$\delta_l$	Longitudinal wavenumber	$\delta_s$	Shear wavenumber
$\omega$	Circular frequency	$f$	Frequency
$f_{\text{cut-on}}$	Cut-on frequency	$f_{\text{comp}}$	Compressional frequency
$f_{\text{thin/thick}}$	Frequency limit of thin plate theory	$f_{\text{coinc}_{\text{thin}}}$	Coincidence frequency of a thin plate
$f_{\text{coinc}_{\text{thick}}}$	Coincidence frequency of a thick plate	$f_{\text{crit}_{\text{thin}}}$	Critical frequency of a thin plate
$f_{\text{crit}_{\text{thick}}}$	Critical frequency of a thick plate	$f_{\text{plate/solid}_{\text{oi}}}$	Frequency limit of plate theories for oblique incidence
$f_{\text{plate/solid}_{\text{df}}}$	Frequency limit of plate theories for diffuse field	$c_0$	Speed of sound in the air
$V^P$	State vector of a plate	$V^{ES}$	State vector of an elastic layer
$p$	Pressure at a point	$u$	Transverse velocity at a point
$v$	Normal velocity at a point	$\sigma_{zz}$	Normal stress at a point
$\sigma_{xz}$	Shear stress at a point	$[T^P]$	Transfer matrix of a plate
$[T^{ES}]$	Transfer matrix of an elastic layer	$m_s$	Mass density per unit area
$\rho$	Volume density of elastic layer	$\rho_0$	Volume density of air
$D$	Bending stiffness	$E$	Young's modulus
$K$	Compressional modulus	$\eta$	loss factor
$\nu$	Poisson's ratio	$G$	Shear modulus
$G^*$	Corrected shear modulus	$\kappa$	Shear correction factor
$I_z$	Mass moment of inertia	$\lambda, \mu$	Lamé coefficients
$\tau$	Transmission factor	$Z_P$	Anti-symmetric impedance of a plate
$Z_s$	Symmetric impedance	$Z_a$	Anti-symmetric impedance
$Y_s$	Symmetric admittance	$Y_a$	Anti-symmetric admittance
$\tilde{Y}_s$	Approximated symmetric admittance	$Z_0$	Characteristic impedance of air
$C_k$	Ratio between bending and shear wavenumbers	$C_y$	Minimum value of ratio between anti-symmetric and symmetric admittances
$\epsilon$	Error percentage	$\lambda_l$	Longitudinal wavelength

16 **1. Introduction**

17 When studying the sound insulation of a wall, the main acoustic indi-  
 18 cator is the transmission loss (TL) which is controlled by the combination  
 19 of several fundamental vibrating modes of the wall. For example, a typical  
 20 sound transmission problem encountered in building applications is presented  
 21 schematically in Fig. 1 [along with its vibrating modes as the acoustic energy](#)  
 22 [transmitted through the wall depends on its vibro-acoustic behaviour](#). Al-  
 23 though the wall vibrates in a complex manner for the given acoustic excita-  
 24 tion, this complex motion can be obtained by superposing the fundamental

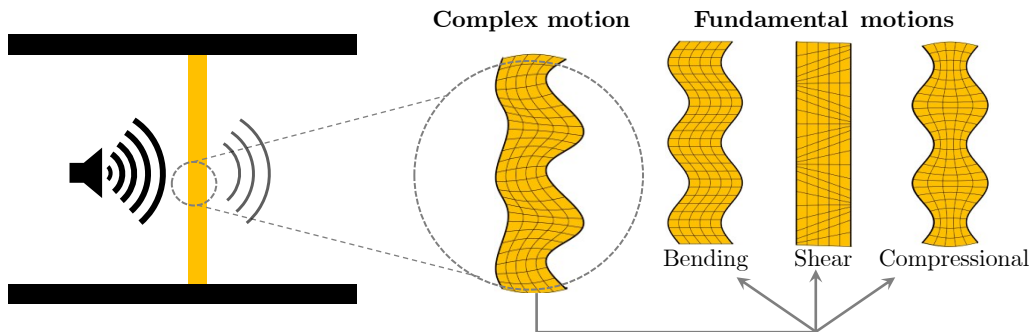


Figure 1: Schematic representation of vibrating motion of a single wall subjected to acoustic excitation.

25 motions (bending, shear and compressional/dilatational motions). Generally,  
 26 looking at the TL characteristics of a single wall as a function of frequency,  
 27 three regions can be identified which are controlled by the mass, damping  
 28 and stiffness of the wall respectively. The mass and stiffness control zones are  
 29 separated by a critical region where strong reduction of transmission loss is  
 30 observed. This critical zone is characterized by its frequency which is called  
 31 the critical frequency. Various vibro-acoustic models of varying complexity  
 32 have been developed to predict the sound insulation properties of plate structures,  
 33 especially with regard to noise attenuation problems. An early model  
 34 was developed by Cremer [1] which was applied to the computation of the  
 35 TL across infinite, thin walls. Related work approaching the same problem  
 36 of computing the acoustic insulation indicators of a thin wall are presented  
 37 in [2–6]. In Cremer’s model, it is assumed that the motion of the plate is  
 38 described only by the bending wave equation, which is based on the classical  
 39 plate theory [7].

40 Davy [8] argues that Cremer’s model can only be used below the critical  
 41 frequency since most of the approximations are not valid within and above  
 42 the critical region. Improving on Cremer’s theory, Heckl and Donner [9] developed  
 43 a model based on the first order shear deformation theory (FSDT)  
 44 [10–12] which could be applied to thicker walls to compute sound TL. In  
 45 this model, motion due to the transverse shear is also included along with the  
 46 flexural motion of the plate. The corrected TL expression accounting for  
 47 shear deformation of the plate can be found in [13]. Heckl and Donner [9]  
 48 point out that their model is valid only at frequencies well below the first  
 49 dilatational or compressional frequency of the plate. This is due to the fact  
 50 that the FSDT does not account for the thickness stretch motion of the plate  
 51 as it assumes constant velocity at all points through the thickness direction.  
 52 Consequently, the symmetric motion of the plate is not taken into account

53 in zero, first and higher order plate theories. This may lead to deviations  
54 between the predictions and the actual motion of the plate at higher frequen-  
55 cies, especially when the material is soft. In the work published by Ljunggren  
56 [13, 14], the general expression to compute the TL of an infinite wall with  
57 arbitrary uniform thickness is given, accounting for both antisymmetric and  
58 symmetric motions of the plate.

59 In recent years, instead of single wall structures, multi-layered struc-  
60 tures have been used widely for better sound comfort and noise attenua-  
61 tion. These structures provide the designers with more choices for tuning  
62 the vibro-acoustic performance leading to better sound insulation character-  
63 istics. Advanced composite structures are one example of multi-layer systems  
64 that are progressively used in different fields such as the space, energy and  
65 aeronautical industries. In transport and construction industries, sandwich  
66 structures are widely used as they provide high stiffness with significantly  
67 low weight. In most cases, two face sheets are bonded with a viscoelastic  
68 layer to improve the overall damping response of the structure. There exist a  
69 large number of theoretical models dedicated to the analysis of the behaviour  
70 of multi-layer structures. According to Carrera [15, 16], these models can be  
71 classified into three major categories as: 1) Equivalent Single Layer (ESL)  
72 models, 2) Layer Wise (LW) models and 3) Hybrid or Zig-Zag models. ESL  
73 models describe the dynamics of the multi-layer plate in terms of the dis-  
74 placement field of an equivalent layer. It is noted that, due to this kind  
75 of displacement description, the number of layers present in the system do  
76 not influence the displacement functions which gives great flexibility in using  
77 shear deformation theories of order one [10–12] and higher [17–20]. Layer  
78 Wise (LW) models describe the displacement field in each layer [21–28]; as  
79 a consequence, this type of model requires higher computational effort as  
80 the number of unknowns increases with the number of layers present in the  
81 structure. Hybrid or Zig-Zag models make use of advantages from the previ-  
82 ous two categories. Although the displacement field is defined in each layer  
83 (similar to the LW models), the interface continuity conditions between two  
84 adjacent layers results in a lower number of unknown functions (as in ESL  
85 models) which do not depend on the number of layers present in the struc-  
86 ture. The reader may refer to [29–34] which use this family of models to  
87 describe the dynamic response of multi-layer systems.

88 Since industrial multi-layer structures are manufactured with a diversity  
89 of materials, they naturally increase the computational burden for detailed  
90 finite element modelling and it is therefore of interest to condense the be-  
91 haviour of the multi-layer system into a single layer. A simplified equivalent  
92 thin plate model was developed in [35–37] for sandwich structures with a  
93 viscoelastic core. Guyader and Cacciolati [38] have developed an equivalent

94 thin plate model for the multi-layer structure of isotropic layers. Following  
95 a similar path, Marchetti et al. [39] have recently developed an equivalent  
96 thin plate model for laminated structures of orthotropic layers. The aim of  
97 the equivalent plate models is to find the frequency dependent mechanical  
98 parameters of the equivalent thin plate that incorporates the bending and  
99 shear motions of the multi-layer structures. Since plate theories do not ac-  
100 count for the dilatational or compressional motion of the structure, finding a  
101 frequency domain of validity is necessary to safely use these equivalent plate  
102 models.

103 The reader may note that the words ‘frequency limit’ of a theory refer here  
104 to the frequency up to which the theory can be applied within pre-defined  
105 accuracy intervals for computing the desired acoustic indicators. [Although in  
106 structural mechanics and dynamics, thin and thick plates are distinguished  
107 based on the thickness to lateral dimensions ratio \[40, 41\], such rules may not  
108 be sufficient for vibro-acoustic calculations as they depend on the material  
109 properties of the plate as well.](#) Additionally, although plate theories (both  
110 for thin and thick plates) are commonly employed in computing the acoustic  
111 indicators of infinite and finite walls, there is currently no clear-cut frequency  
112 limit to restrict the applicability of these theories. Qualitative and approxi-  
113 mate frequency limits are given in the literature but it is often a tedious task  
114 to find an analytical expression for applicability limits.

115 In this work, we derive for the first time analytical expressions for the  
116 applicability limits in the spectral domain for thin and thick plate theories.  
117 Through analysis of the propagating wavenumbers and admittances of the  
118 investigated panels, we quantify the expected accuracy of each theory. The  
119 paper is organized as follows: Sec. 2 describes the theories behind propagating  
120 wavenumbers inside thin, thick plates and elastic solids. The theory of elastic  
121 solids is treated as a reference since it describes the complete motion of an  
122 infinite layer [42]. In Sec. 3, expressions for the limits of applicability of thin  
123 plate theories are discussed by comparing propagating wavenumbers of thin  
124 and thick plate theories. Additionally, refined expressions for the coincidence  
125 and critical frequencies are also presented. In Sec. 4, an expression for the  
126 frequency limit of applicability of plate theories is derived in all generality by  
127 comparing the order of magnitudes of both symmetric and anti-symmetric  
128 admittances of the plate. In Sec. 5, analytical expressions for the frequency  
129 limits of different plate theories are presented along with sound transmission  
130 loss computations for classical industrial materials for validation purposes.

131 **2. Vibro-acoustic models for an elastic isotropic layer**

132 We start by giving the theoretical background for some commonly used  
 133 theories such as the Love-Kirchoff [7, 43] or the Reissner-Mindlin [10–12]  
 134 theory used to describe the vibro-acoustic behaviour of isotropic, single wall  
 135 structures. In subsequent sections, these theories are compared and their  
 136 limitations are discussed.

137 *2.1. Wave propagation in an elastic isotropic plate*

138 Let us consider an infinitely extended elastic medium with thickness  $h$   
 139 as shown in Fig. 2. An oblique wave is assumed to be impinging upon one  
 140 of the surfaces of the elastic medium with an incident angle  $\theta$ . For the sake  
 141 of simplicity, the incident plane wave is assumed to be in the  $x - z$  plane.  
 Depending on the material properties of the elastic layer, various types of

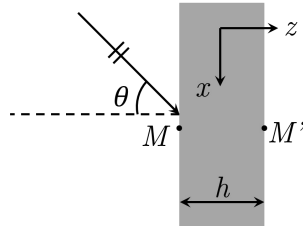


Figure 2: An oblique plane wave impinging on an infinitely extending elastic isotropic layer with incident angle  $\theta$ .

142 wave propagation are possible. The wave propagation in the  $x - z$  plane  
 143 will have wave vector components along the  $x$  and  $z$  axes for each wave.  
 144 The incident wave in free air is exciting waves inside the elastic medium;  
 145 continuity across the interface demands that the transverse or  $x$  component  
 146 of the wave vector,  $k_t$ , for waves propagating in the plate and in air are equal.  
 147 We have

$$k_t = k_0 \sin \theta = \frac{\omega}{c_0} \sin \theta, \quad (1)$$

149 where  $k_0$  is the wavenumber in free air,  $\omega = 2\pi f$  is the circular frequency of  
 150 the incident wave and  $c_0$  is the speed of sound in air. If the acoustic field in  
 151 the elastic layer (Fig. 2) is described by the state vector  $V^P = \{p, v\}^T$  (where  
 152 the superscript  $P$  denotes plate,  $p$  is the acoustic pressure and  $v$ , the particle  
 153 velocity normal to the interface), then the general form of the transfer matrix  
 154 for plate theories discussed can be expressed by the following equation:

$$V_M^P = [T^P] V_{M'}^P = \begin{bmatrix} 1 & Z_P \\ 0 & 1 \end{bmatrix} V_{M'}^P. \quad (2)$$

155 Here,  $M$  and  $M'$  are points on the left and right hand side on the surface  
 156 of the elastic medium, respectively and  $Z_P$  is the anti-symmetric mechanical  
 157 impedance of the plate, that is, the ratio of the differential complex sound  
 158 pressure across the plate to the complex plate velocity; it is expressed as  
 159 below based on the theory adopted, that is,

$$Z_P = \begin{cases} Z_{thin} = j\omega m_s \left(1 - \frac{Dk_t^4}{\omega^2 m_s}\right) \\ Z_{thick} = \frac{k_t^4 D - m_s \omega^2 + \left(\frac{I_z m_s}{G^* h} \omega^2 - k_t^2 \frac{D m_s}{G^* h}\right) \omega^2 - k_t^2 I_z \omega^2}{j\omega \left(\frac{k_t^2 D - I_z \omega^2}{G^* h} + 1\right)} \end{cases}, \quad (3)$$

160 where Love-Kirchoff theory applies for thin plates and Reissner-Mindlin the-  
 161 ory for thick plates. Here,  $m_s$  is the mass density per unit area,

$$D = \frac{E(1 + j\eta)h^3}{12(1 - \nu^2)}$$

162 is the bending stiffness,  $E$  is the Young's modulus,  $j = \sqrt{-1}$ ,  $\eta$  is the  
 163 loss/damping factor,  $\nu$  is the Poisson's ratio,  $G^* = \kappa G$  with  $G$ , the shear  
 164 modulus of the plate and  $\kappa$ , the shear correction factor accounting for the  
 165 transverse shear distribution. Furthermore,

$$I_z = \frac{\rho h^3}{12}$$

166 is the mass moment of inertia of the plate and  $\rho = m_s/h$  is the volume density  
 167 of the plate material. Detailed derivations of the mechanical impedances  
 168 given in Eq. (3) can, for example, be found in the book by Cremer and Heckl  
 169 [44].

170 When using the thick plate theory, the shear correction factor,  $\kappa$ , is sub-  
 171 stituted with different values/expressions by different authors. For example,  
 172 Reissner [11] and Mindlin [10] used the values  $5/6$  and  $\pi^2/12$ , respectively, for  
 173 the shear correction factor, whereas Heckl and Donner [9] used the following  
 174 expression given by Magrab [45],

$$\kappa = \left(\frac{0.87 + 1.12\nu}{1 + \nu}\right)^2$$

175 which is a function of the Poisson's ratio of the plate. In this article, the  
 176 value of  $\kappa$  is taken as  $5/6$ .

177 *2.1.1. Dispersion relations*

178 Given the mechanical impedances of the structure, dispersion relations are  
 179 often obtained by setting the impedance to zero. In other words, dispersion  
 180 relations are used to understand the wave propagation in the structure under  
 181 natural or free vibration conditions.

182 For Love-Kirchoff plates (or thin plates), by setting the mechanical impedance  
 183 equal to zero, it can be observed that only one type of wave propagation is  
 184 possible, that is,

$$Z_{thin} = 0 \Rightarrow k_p^4 D - m_s \omega^2 = 0 \Rightarrow k_p = k_b = \sqrt{\omega \sqrt{\frac{m_s}{D}}}, \quad (4)$$

185 where  $k_b$  corresponds to the bending wavenumber and  $k_p$  is the natural prop-  
 186 agating wavenumber of the plate.

187 For Reissner-Mindlin plates (or thick plates), the dispersion relation is  
 188 obtained as

$$Z_{thick} = 0 \Rightarrow k_p^4 D - m_s \omega^2 + \left( \frac{I_z m_s}{G^* h} \omega^2 - k_p^2 \frac{D m_s}{G^* h} \right) \omega^2 - k_p^2 I_z \omega^2 = 0. \quad (5)$$

189 There are four possible solutions for the above quartic equation, that is,

$$k_p = \pm \sqrt{\frac{m_s \omega^2}{2G^* h} + \frac{I_z \omega^2}{2D}} \pm \sqrt{\frac{m_s \omega^2}{D} + \left( \frac{m_s \omega^2}{2G^* h} - \frac{I_z \omega^2}{2D} \right)^2}. \quad (6)$$

190 Out of the four solutions, two correspond to outgoing waves, that is, the real  
 191 part of the wavenumber is positive; these are

$$k_p = k_{RM_{1,2}} = \sqrt{\frac{m_s \omega^2}{2G^* h} + \frac{I_z \omega^2}{2D}} \pm \sqrt{\frac{m_s \omega^2}{D} + \left( \frac{m_s \omega^2}{2G^* h} - \frac{I_z \omega^2}{2D} \right)^2}. \quad (7)$$

192 It is observed from the above equation that the propagating wavenumber  
 193 ( $k_{RM_1}$ ) has different asymptotic behaviour with respect to low and high fre-  
 194 quencies as shown in Fig. 3, here for the example of a **50 mm** plasterboard  
 195 with mechanical properties listed in Table 1. One finds in particular:

196 – At low frequency (or  $\omega \rightarrow 0$ ), we have

$$\frac{m_s}{D} \gg \left( \frac{m_s}{2G^* h} - \frac{I_z}{2D} \right)^2 \omega^2$$

197 which results in  $k_{RM_1}$  tending to  $k_b$

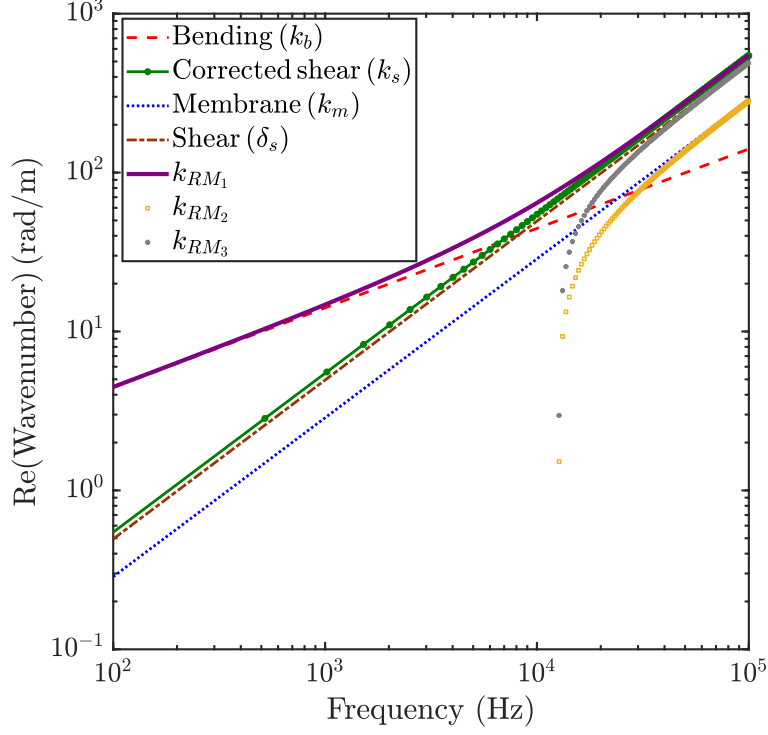


Figure 3: Propagating wavenumbers of a Reissner-Mindlin plate (50 mm plasterboard with mechanical properties mentioned in Table 1) and its asymptotic behaviours. It is observed that the main natural propagating wavenumber  $k_{RM_1}$  is approaching bending ( $k_b$ ) and corrected shear wavenumbers ( $k_s$ ) at low and high frequencies respectively.

198 – At high frequency (or  $\omega \rightarrow +\infty$ ), we find

$$\frac{m_s}{D} \ll \left( \frac{m_s \omega^2}{2G^*h} - \frac{I_z}{2D} \right)^2 \omega^2$$

199 which results in  $k_{RM_1}$  tending to  $k_s = \omega \sqrt{\frac{m_s}{G^*h}}$  with  $k_s$ , the corrected  
200 shear wavenumber.

201 –  $k_{RM_2}$  is evanescent until the cut-on frequency given by Eq. (9) after  
202 which it becomes propagating and reaches the membrane wavenumber

203  $k_m = \omega \sqrt{\frac{I_z}{D}}$  at high frequency.

204 –  $k_s$  is always greater than  $k_m$  since  $\frac{k_s}{k_m} = \sqrt{\frac{2}{\kappa(1-\nu)}} > 1$

205 Based on the above observations, Eq. (7) is rewritten in a compact form as,

$$k_{RM_{1,2}} = \sqrt{\frac{1}{2} \left[ k_s^2 + k_m^2 \pm \sqrt{4k_b^4 + (k_s^2 - k_m^2)^2} \right]}. \quad (8)$$

206 The cut-on frequency can be obtained by considering  $k_{RM_2} = 0$ , that is,

$$k_s^2 + k_m^2 = \sqrt{4k_b^4 + (k_s^2 - k_m^2)^2} \quad \Rightarrow \quad k_b^4 = k_s^2 k_m^2$$

207 and thus

$$f_{\text{cut-on}} = \frac{1}{2\pi} \sqrt{\frac{G^* h}{I_z}}. \quad (9)$$

208 Further, it is observed that the high frequency asymptote given by Ghinet  
209 and Atalla [27] as

$$k_{G\&A} = \omega \sqrt{\frac{4I_z m_s}{G^* h I_z + m_s D}}. \quad (10)$$

210 differs from the correct estimation of the high frequency asymptote  $k_s$ . It  
211 may be noted that Eq. (5) can be obtained from two of the three equilibrium  
212 equations (derived by a Newtonian approach) for thick plates [46]. For the  
213 sake of completeness, the dispersion relation resulting from third equilibrium  
214 equation [27] is presented here. The natural wavenumber from the third  
215 equilibrium equation is given by,

$$k_p = k_{RM_3} = \sqrt{\frac{2}{1-\nu} \frac{I_z \omega^2 - G^* h}{D}} = \sqrt{\delta_s^2 - \frac{2}{1-\nu} \frac{k_b^4}{k_s^2}}, \quad (11)$$

216 where  $\delta_s = \omega \sqrt{\frac{\rho}{G}}$  is the pure shear wavenumber of the isotropic elastic layer.

217 Similar to  $k_{RM_2}$ ,  $k_{RM_3}$  is also evanescent until a cut-on frequency ( $f_{\text{cut-on}}$ ) but  
218 reaches the asymptote  $\delta_s$  at higher frequencies as

$$\delta_s^2 \gg \frac{2}{1-\nu} \frac{k_b^4}{k_s^2}$$

219 when  $\omega \rightarrow +\infty$ . Fig. 3 illustrates these asymptotic behaviours of the solu-  
220 tions of  $k_{RM}$  for a plasterboard of thickness **50 mm**. Mechanical properties  
221 of the materials used in this paper can be obtained from Table 1.

222 The transmission loss across an infinite layer surrounded by air (defined  
223 by the equation  $V_M = [T]_{2 \times 2} V_{M'}$ ) for an oblique incidence may be computed  
224 from the following expression:

$$\text{TL} = -10 \log_{10} \tau, \quad (12)$$

Table 1: Material properties of few typical elastic isotropic layers used in this paper

Properties	Aluminium	Plasterboard	Concrete	Soft layer
$\rho$ (kg/m <sup>3</sup> )	2780	700	2150	8
$E$ (GPa)	71	3	33	0.00016
$\eta$	0.01	0.08	0.1	0.1
$\nu$	0.3	0.22	0.23	0.44

225 where

$$\tau(\theta) = 4 / \left| T_{11} + T_{22} - \left( \frac{T_{12} \cos \theta}{Z_0} + \frac{T_{21} Z_0}{\cos \theta} \right) \right|^2$$

226 is the transmission factor,  $Z_0 = \rho_0 c_0$  is the characteristic impedance of air  
 227 and  $\rho_0$  is the density of air. In this paper, the values for  $c_0$  and  $\rho_0$  are taken  
 228 as 343 m.s<sup>-1</sup> and 1.2 kg.m<sup>-3</sup>, respectively. The reader may note that for  
 229 plate theories, the transmission factor is reduced to the form

$$\tau(\theta) = 1 / \left| 1 + \frac{Z_P \cos \theta}{2Z_0} \right|^2.$$

230 In case of a diffuse field excitation with minimum and maximum angle of  
 231 incidences as  $\theta_{\min}$  and  $\theta_{\max}$ , respectively, the TL is obtained computing the  
 232 following integral:

$$\text{TL}_d = -10 \log_{10} \left[ \frac{\int_{\theta_{\min}}^{\theta_{\max}} \tau(\theta) \sin \theta \cos \theta, d\theta}{\int_{\theta_{\min}}^{\theta_{\max}} \sin \theta \cos \theta, d\theta} \right]. \quad (13)$$

233 TL computed based on both thin and thick plate theories for the materials  
 234 given in Table 1, are analyzed in the Section 5.

235 It must be realized that both thin and thick plate theories neglect the  
 236 compressional mode (also called the symmetric or dilatational mode) and  
 237 allow only anti-symmetric modes (i.e, bending and/or shear modes), since  
 238 the plate velocity is assumed to be constant through the thickness direction.

## 239 2.2. Wave propagation in elastic isotropic solids

240 From the principles of the theory of elasticity, it can be derived that two  
 241 fundamental waves can propagate through an isotropic medium correspond-  
 242 ing to longitudinal and shear displacement in the solid. Longitudinal ( $\delta_l$ )

243 and shear ( $\delta_s$ ) wave numbers are given as [42],

$$\delta_l = \omega \sqrt{\frac{\rho}{\lambda + 2\mu}} = \omega \sqrt{\frac{\rho}{K}}, \quad \delta_s = \omega \sqrt{\frac{\rho}{\mu}}, \quad (14)$$

244 where  $K = \lambda + 2\mu$  is the compressional modulus of the elastic solid which  
245 highly influences the symmetric motions of the layers in a solid,

$$\lambda = \frac{E\nu}{(1 + \nu)(1 - 2\nu)}$$

246 is the first Lamé coefficient and  $\mu = G$  is the second Lamé coefficient.

247 Assuming an acoustic wave incident on the surface of the solid with angle  
248  $\theta$ , the resulting wavenumbers that propagate inside the elastic solid have a  $z$   
249 component of the form,

$$k_{lz} = \sqrt{\delta_l^2 - k_t^2}, \quad k_{sz} = \sqrt{\delta_s^2 - k_t^2}. \quad (15)$$

250 By following Folds and Loggins [47], the state vector is taken as  $V^{ES} =$   
251  $\{u, v, \sigma_{zz}, \sigma_{xz}\}^T$  where the superscript ES denotes elastic solid,  $\sigma_{xz}$  and  $u$  are  
252 the transverse components of the stress and the velocity, and  $\sigma_{zz}$  and  $v$  the  
253 normal components of the stress and the velocity respectively. The transfer  
254 matrix for elastic solid is then expressed as

$$V_M^{ES} = [T^{ES}]_{4 \times 4} V_{M'}^{ES}, \quad (16)$$

255 where the elements of the matrix  $[T^{ES}]$  are given in the Appendix A. For  
256 the computation of sound transmission loss across an infinite layer based on  
257 the solid transfer matrix, the reader may refer to the procedure given in the  
258 book by Allard and Atalla [42].

259 Based on the type of backing at point  $M'$ , the frequency of the first  
260 compressional mode of an elastic layer is given as

$$f_{\text{comp}} = \frac{1}{\gamma h} \sqrt{\frac{K}{\rho}}, \quad (17)$$

261 where  $\gamma$  takes on the values 2 (half wave frequency) and 4 (quarter wave  
262 frequency) for anechoic and rigid backing respectively.

263 Since the motion both of the anti-symmetric and compressional mode of  
264 an infinite layer of finite thickness can be expressed based on the theory of  
265 elasticity, calculations of the transfer matrix for elastic solids are considered  
266 here as reference to the analyse using plate theories. By referring to the two  
267 fundamental wavenumbers ( $\delta_l$  and  $\delta_s$ ) of the elastic isotropic solid, it can be  
268 understood that the bending wavenumber is a complex combination of these  
269 fundamental wavenumbers. It is, however, not straightforward to see this  
270 relation from the above equations for elastic isotropic solids.

### 271 3. Comparison between thin and thick plate theories

#### 272 3.1. Frequency limit of thin plate theory in comparison with thick plate theory

273 In this section, natural propagating wavenumbers of thin and thick plate  
 274 theories are used to find the frequency limit of the thin plate theory. From  
 275 the Fig. 3, it can be seen that the thick plate wavenumber ( $k_{RM_1}$ ) clearly  
 276 deviates from the bending wavenumber ( $k_b$ ) after certain frequency. It may  
 277 be noted that, though there are totally three outgoing waves characterized by  
 278 wavenumbers ( $k_{RM_1}, k_{RM_2}$  &  $k_{RM_3}$ ),  $k_{RM_1}$  is considered for the present anal-  
 279 ysis as it is the only wavenumber that is always propagative. Additionally,  
 280 since the deviation between  $k_{RM_1}$  and  $k_b$  starts well before the cut-on fre-  
 281 quency ( $f_{\text{cut-on}}$ ),  $k_{RM_1}$  would be appropriate to derive the frequency limit of  
 282 thin plate theory. By defining  $C_k = \frac{k_b}{k_s}$ , the ratio between bending and shear  
 283 wavenumbers, error percentage ( $\epsilon$ ) between the propagating wavenumbers of  
 284 the thin and thick plate theories is expressed as

$$\epsilon = \left(1 - \frac{1}{k_{RM_1}/k_b}\right) 100\%, \quad (18)$$

285 where

$$\frac{k_{RM_1}}{k_b} = \frac{1}{2} \sqrt{\frac{2 + \kappa(1 - \nu)}{C_k^2} + \sqrt{16 + \left[\frac{2 - \kappa(1 - \nu)}{C_k^2}\right]^2}}. \quad (19)$$

286 The thin plate theory will be valid while  $k_s$  is negligible compared to  $k_b$   
 287 ( $k_b \gg k_s$ ). The value for  $C_k$  can be chosen such that  $\epsilon$  is below an accepted  
 288 error percentage and the frequency range of validity for thin isotropic plate  
 289 can be expressed as given by Eq. (20).

$$k_b \geq C_k k_s \Rightarrow f \leq f_{\text{thin/thick}} = \frac{G^* h}{2\pi C_k^2} \sqrt{\frac{1}{m_s D}} = \frac{\kappa}{4\pi h C_k^2} \sqrt{\frac{12E}{\rho} \frac{1 - \nu}{1 + \nu}}, \quad (20)$$

290 where  $f_{\text{thin/thick}}$  is the frequency limit of the ‘thin’ plate theory by keeping the  
 291 ‘thick’ plate theory as reference. For instance, choosing  $C_k = 4$  for typical  
 292 isotropic layer corresponds to an error percentage ( $\epsilon$ ) around 2% between  
 293  $k_{RM_1}$  and  $k_b$ .

#### 294 3.2. Coincidence and critical frequencies of thick plate

295 As discussed in the earlier sections, thin plate theory allows only bending  
 296 waves to propagate in the elastic plate and shear wave propagation is in-  
 297 cluded by thick plate theory to correctly capture the anti-symmetric motion  
 298 of the plate. Due to this additional anti-symmetric motion in the plate, the

299 coincidence and critical frequency expressions obtained from thin plate the-  
 300 ory need to be rewritten with terms corresponding to shear and rotational  
 301 inertia.

302 The coincidence frequency between a plate and an acoustic wave incident  
 303 on the plate at an angle  $\theta$  is defined as the frequency at which the transverse  
 304 component of the incident wavenumber is equal to the natural propagating  
 305 wavenumber of the plate. In the case of thin plates, the natural propagating  
 306 wavenumber is the bending wavenumber and the coincidence frequency is  
 307 expressed as,

$$k_b = k_0 \sin \theta \implies f_{\text{coinc}_{\text{thin}}} = \frac{1}{2\pi} \left( \frac{c_0}{\sin \theta} \right)^2 \sqrt{\frac{m_s}{D}}. \quad (21)$$

308 For thick plates, as the natural propagating wavenumber is given by  $k_{RM_1}$ ,  
 309 the coincidence frequency is expressed as,

$$k_{RM_1} = k_0 \sin \theta \implies f_{\text{coinc}_{\text{thick}}} = \frac{(c_0/\sin \theta)^2}{2\pi \sqrt{\left( \frac{D}{m_s} - \frac{c_0^2}{\sin^2 \theta} \frac{I_z}{m_s} \right) \left( 1 - \frac{c_0^2}{\sin^2 \theta} \frac{m_s}{G^* h} \right)}}. \quad (22)$$

310 In case of diffuse field excitation, the elastic layer is subjected to all coinci-  
 311 dence frequencies corresponding to  $\theta = [0, \pi/2]$  and the lowest coincidence  
 312 frequency is called the critical frequency. In other words, it is the frequency  
 313 at which the speed of sound is equal to the speed of natural propagating  
 314 waves of the plate. This can be computed by letting  $\sin \theta = 1$  in the coinci-  
 315 dence frequency expression. The critical frequency obtained from thin plate  
 316 theory is given by  $k_b = k_0$ , that is,

$$f_{\text{crit}_{\text{thin}}} = \frac{c_0^2}{2\pi} \sqrt{\frac{m_s}{D}}. \quad (23)$$

317 From the Eq. (22), the critical frequency for thick plate is obtained from  
 318  $k_{RM_1} = k_0$ , that is,

$$f_{\text{crit}_{\text{thick}}} = \frac{c_0^2}{2\pi \sqrt{\left( \frac{D}{m_s} - c_0^2 \frac{I_z}{m_s} \right) \left( 1 - c_0^2 \frac{m_s}{G^* h} \right)}}. \quad (24)$$

319 It may be noted that the Eqs. (22) and (24) tend to coincidence and critical  
 320 frequencies obtained from thin plate theory as  $I_z \rightarrow 0$  and  $G^* \rightarrow \infty$ . As an  
 321 illustration, for 12.5 mm plasterboard, the coincidence frequencies computed

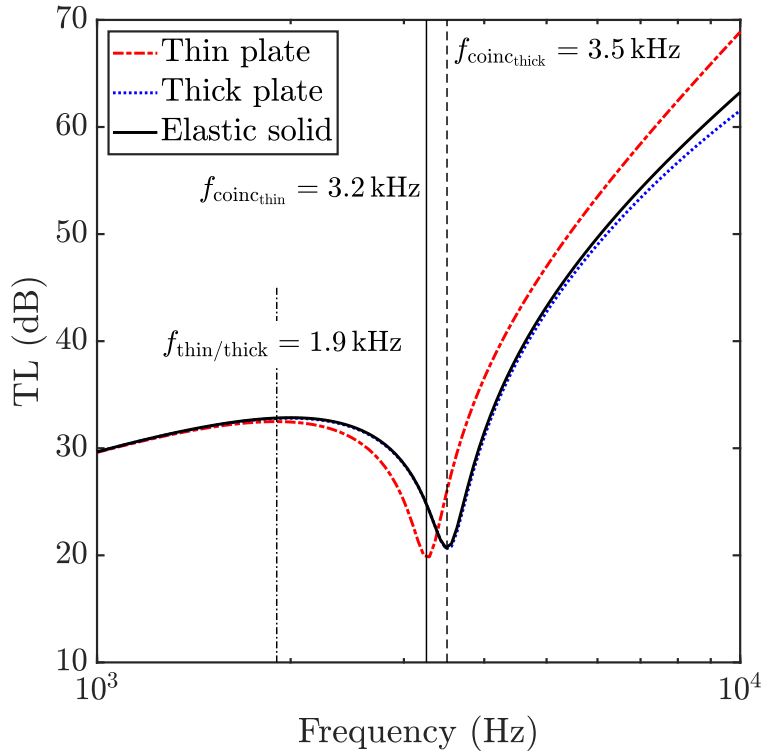


Figure 4: Transmission loss for the infinitely extent plasterboard of thickness 12.5 mm (properties are mentioned in Table 1) under plane wave excitation with  $\theta = 60^\circ$  with coincidence frequencies computed from thin & thick theories and it can be observed that the estimation of coincidence frequency from thick plate theory is in good agreement with theory of elasticity computation.

322 from both plate theories are indicated in the Fig. 4. It is observed from the  
 323 Fig. 4 that the coincidence frequency computed from Eq. (22) is in good  
 324 agreement with elasticity theory. Therefore, it is worth noting that Eqs. (21)  
 325 and (23) are indeed limited to thin plates only, where the transition from  
 326 thin to thick plates is given by the frequency  $f_{\text{thin/thick}}$  in Eq. (20).

#### 327 4. Frequency limit of plate theories in comparison with theory of 328 elasticity

329 When the thickness of the layer is small compared to the lateral dimension  
 330 and the longitudinal wavelength ( $\lambda_l = 2\pi/\delta_l$ ) is large compared to thickness,  
 331 a plate theory, controlled by the anti-symmetric motion, is generally con-  
 332 sidered. On the contrary, when the thickness of the plate is of the order

333 of magnitude of longitudinal wavelength, due to the variation in velocity  
 334 through the thickness of the layer, both symmetric and anti-symmetric motions  
 335 contribute for the resulting motion of the plate after a certain frequency  
 (Fig. 5). This implies that plate theories might not be able to predict the



Figure 5: Vibrating modes of an infinitely extent elastic layer. While the symmetric mode corresponds to the thickness stretch motion of the layer where the particle velocity varies through the thickness, the anti-symmetric motion corresponds to the bending and shear motions of the layer where the particle velocity is constant through the thickness.

336  
 337 correct vibro-acoustic behaviour of the elastic layer after this frequency as  
 338 they assume only anti-symmetric motions in the plate. Therefore, finding  
 339 this frequency limit of plate theories is necessary and in this section, based  
 340 on the symmetric and anti-symmetric motions of the plate, the analytical  
 341 expression of the frequency limit of plate theories is derived.

342 Contributions of symmetric and anti-symmetric motions of an isotropic  
 343 layer can be quantified by the impedances or admittances, by following Dym  
 344 and Lang [48]. Impedances of symmetric and anti-symmetric motions are  
 345 defined as follows [48],

$$Z_s = 2 \frac{p_M + p_{M'}}{v_M - v_{M'}}, \quad (25)$$

$$Z_a = 2 \frac{p_M - p_{M'}}{v_M + v_{M'}}, \quad (26)$$

347 where  $Z_s$  and  $Z_a$  are symmetric, anti-symmetric impedances of the layer re-  
 348 spectively and  $p$  and  $v$  are pressure and velocity respectively. It may be noted  
 349 that though Dym and Lang [48] assumed  $p_{M'} = 0$  in their analysis, later, they  
 350 have corrected the definitions of impedances with non-zero pressure values  
 351 [49].

352 The above equations are rewritten to obtain the transfer matrix relations  
 353 as follows,

$$\begin{pmatrix} p \\ v \end{pmatrix}_M = \frac{1}{Y_a - Y_s} \begin{bmatrix} Y_a + Y_s & 1 \\ 4Y_a Y_s & Y_a + Y_s \end{bmatrix} \begin{pmatrix} p \\ v \end{pmatrix}_{M'}. \quad (27)$$

354 Here,  $Y_s = 1/Z_s$  and  $Y_a = 1/Z_a$  are the symmetric and anti-symmetric  
 355 admittances of the layer respectively. It can be checked that, when the anti-  
 356 symmetric admittance is larger than the symmetric admittance (or  $Y_a \gg Y_s$ ),  
 357 the transfer matrix in Eq. (27) reduces to the transfer matrix of the plate

358 given by Eq. (2). Thus the ratio between  $Y_a$  and  $Y_s$  could be a good criterion  
 359 to obtain the frequency limit of plate theories. Comparing the longitudinal  
 360 wavelength ( $\lambda_l$ ) to the thickness of the plate seems less accurate as it does  
 361 not compare the symmetric motion to the anti-symmetric motion.

362 Since the symmetric motion is controlled by the longitudinal wave of the  
 363 layer, the transfer matrix from Eq. (16) is deduced at normal incidence as

$$\begin{pmatrix} p \\ v \end{pmatrix}_M = \begin{bmatrix} \cos h\delta_l & \frac{j\omega\rho}{\delta_l} \sin h\delta_l \\ \frac{j\delta_l}{\omega\rho} \sin h\delta_l & \cos h\delta_l \end{bmatrix} \begin{pmatrix} p \\ v \end{pmatrix}_{M'}. \quad (28)$$

364 By equating the above equation with Eq. (27), the symmetric admittance is  
 365 obtained as

$$Y_s = \frac{h\delta_l(\cos h\delta_l - 1)}{2jm_s\omega \sin h\delta_l} = -\frac{h\delta_l}{2jm_s\omega} \tan \frac{h\delta_l}{2}. \quad (29)$$

366 Approximating the tangent function by a Taylor series expansion (up to first  
 367 order), the symmetric admittance can be written as,

$$\tan \frac{h\delta_l}{2} \approx \frac{h\delta_l}{2} \implies Y_s \approx \tilde{Y}_s = -\frac{(h\delta_l/2)^2}{j\omega m_s} = \frac{j\omega h}{4K}. \quad (30)$$

368 Since the anti-symmetric motion is controlled by the transverse wavenum-  
 369 ber of the incident wave and plate theories capture this type of motion, anti-  
 370 symmetric admittance is computed from plate theories as given by Eq. (3).

371 The minimum value of the absolute ratio between the anti-symmetric and  
 372 symmetric admittance, denoted by  $C_y$ , is used to find the frequency limit  
 373 of plate theories. Expressing the anti-symmetric admittance ( $Y_a$ ) from thin  
 374 plate theory and the symmetric admittance ( $\tilde{Y}_s$ ) from Eq. (30), the frequency  
 375 limit of plate theories is expressed as,

$$\left| \frac{Y_a}{\tilde{Y}_s} \right| \geq C_y \implies f \leq f_{\text{plate/solid}_{oi}} = \frac{c_0^2}{2\pi \sin^2 \theta} \sqrt{\frac{m_s}{2D} \pm \sqrt{\left(\frac{m_s}{2D}\right)^2 \pm \frac{4K}{hC_y D} \frac{\sin^4 \theta}{c_0^4}}}. \quad (31)$$

376 The above expression is valid for oblique incidence whereas in case of dif-  
 377 fuse field excitation, the following expression may be used to compute the  
 378 frequency limit of plate theories.

$$\left| \frac{Y_a}{\tilde{Y}_s} \right| \geq C_y \implies f \leq f_{\text{plate/solid}_{df}} = \frac{c_0^2}{2\pi} \sqrt{\frac{m_s}{2D} \pm \sqrt{\left(\frac{m_s}{2D}\right)^2 \pm \frac{4K}{hC_y D} \frac{1}{c_0^4}}}. \quad (32)$$

379 The above frequency limits are computed by keeping the loss factor ( $\eta$ ) to  
 380 be zero. The subscript ‘plate/solid’ in the above equations means that the  
 381 frequency limit is for ‘plate’ theories in general (as even higher order plate  
 382 theories also do not account for symmetric motion) by keeping as a refer-  
 383 ence the theory of ‘elastic solids’. Further, the sub-subscripts ‘oi’ and ‘df’  
 384 correspond to ‘oblique incidence’ and ‘diffuse field’ respectively. It may be  
 385 observed that the relation  $\left| \frac{Y_a}{\widetilde{Y}_s} \right| \geq C_y$  yields four positive roots for the fre-  
 386 quency. Out of these four roots, only the minimum of pure real roots is  
 387 considered for  $f_{\text{plate/solid}_{\text{oi}}}$  and  $f_{\text{plate/solid}_{\text{df}}}$ . It may also be noted that the  
 388 expression for  $f_{\text{plate/solid}_{\text{df}}}$  can be modified in two ways. First, by including  
 389 higher order terms for the tangent function to get  $\widetilde{Y}_s$ . Second, by using  
 390 the anti-symmetric mechanical admittance from thick plate theory. Though  
 391 these two ways might improve the frequency limit, the final expression for  
 392  $f_{\text{plate/solid}_{\text{df}}}$  would become more complex. Further, as discussed in the next  
 393 section, the frequency limits given by Eqs. (31) and (32) are sufficient enough  
 394 for typical single layer walls used in industry. A concrete layer of 140 mm  
 395 is taken to illustrate the nature of the symmetric and anti-symmetric admit-  
 396 tances of the elastic layer and presented in the Fig. 6.

397 From the Fig. 6, it can be seen that the anti-symmetric admittance is  
 398 larger compared to the symmetric admittance at low frequency range. The  
 399 symmetric admittance is seen to become of the same order of magnitude  
 400 or larger compared to the anti-symmetric impedance at around 2000 Hz.  
 401 By letting the factor  $C_y$  to be 10, the frequency limit of plate theories is  
 402 computed from Eq. (32). This means that the anti-symmetric admittance is  
 403 one order of magnitude larger than the symmetric admittance and from this  
 404 frequency onwards use of plate theories is not recommended to compute the  
 405 acoustic indicators. Therefore, it is advisable to adopt the theory of elasticity  
 406 for computations after this frequency limit.

## 407 5. Numerical examples

408 In this section, transmission loss (TL) of different material layers (with  
 409 properties listed in Table 1) are presented to illustrate the frequency limits  
 410 obtained in sections 3 and 4. Both, oblique plane wave incidence of  $60^\circ$  and  
 411 diffuse fields, are used to compute TL. Since  $f_{\text{plate/solid}_{\text{df}}}$  is the minimum of all  
 412 the possible coincidence frequencies obtained from  $f_{\text{plate/solid}_{\text{oi}}}$ , in this section,  
 413  $f_{\text{plate/solid}_{\text{df}}}$  is indicated as the limit of plate theory. [Though elasticity theory](#)  
 414 [is considered as reference to analyse the plate theories, additional validation](#)  
 415 [from finite element method \(FEM\) is also presented in some of the TL plots](#)  
 416 [in this section.](#)

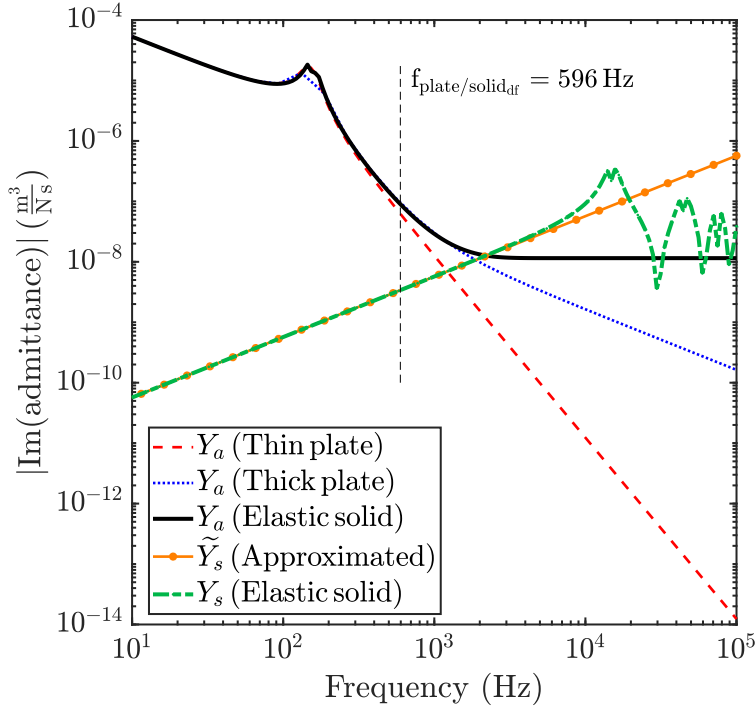


Figure 6: Admittances of a concrete layer of thickness 140 mm (properties are mentioned in Table 1) under plane wave excitation with  $\theta = 60^\circ$ . It is observed that, from low frequencies till the limiting frequency ( $f_{\text{plate/solid}_{\text{df}}}$ ), the symmetric admittance is lesser compared to the anti-symmetric admittance which supports the applicability of plate theories till  $f_{\text{plate/solid}_{\text{df}}}$ .

417 FEM simulations are computed using Comsol Multiphysics© software.  
 418 The acoustical variables (pressure, velocity fields...) are computed in the coupled system (PML-air-material-air-PML) using the “Comsol Pressure Acoustics” interface (Helmholtz equation) for air and “Structural Mechanics branch”  
 419 interface (Helmholtz equation) for air and “Structural Mechanics branch”  
 420 for the material (elastic material in “Solid Mechanic”). The interface between  
 421 air and the material is modeled using “fluid-structure interface”. The dimensions of each material are 60 cm  $\times$  60 cm (the thickness is the real thickness)  
 422 and periodic lateral conditions are chosen. The domain is adjusted (in particular the dimensions of the air domains) and meshed with respect to a  
 423 10 elements per wavelength (of the incident plane wave excitation) criterion  
 424 based on the maximal frequency. For example, at 125Hz, the number of resolved degrees of freedom is 444675, the complete mesh consists of 29889  
 425 domain elements, 8802 boundary elements and 812 edge elements.  
 426  
 427  
 428  
 429

430 In Figs. 7 and 8, TL computed from different theories (discussed in the

431 section 2) are presented for comparison along with frequency limits expressed  
 432 in sections 3 and 4. It is observed from these plots that, for material like  
 433 aluminium (with typical value of thickness used in industries), the thin plate  
 434 theory would be sufficient to model the vibro-acoustic behaviours as both  
 $f_{\text{thin/thick}}$  and  $f_{\text{plate/solid}_{\text{df}}}$  are spotted near the maximum audible frequency.

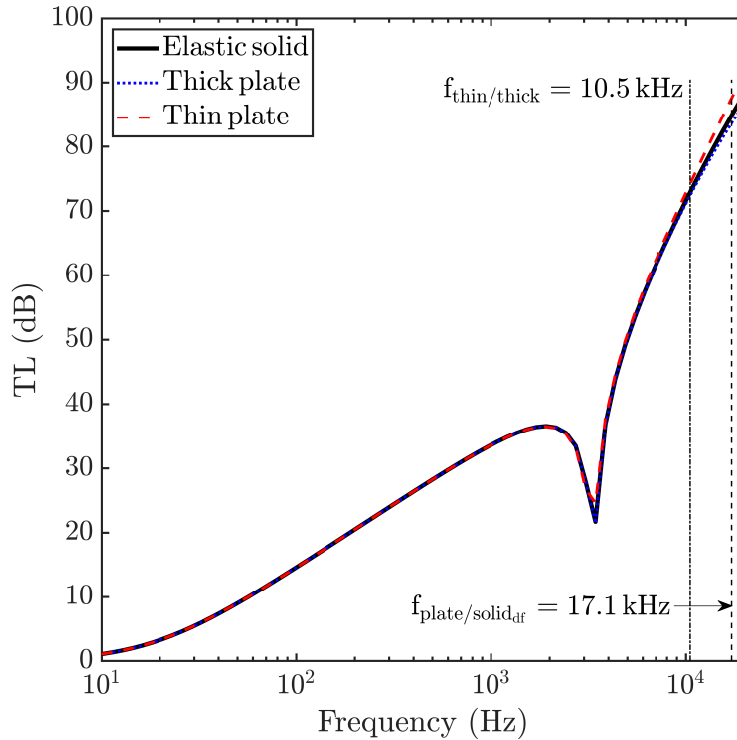


Figure 7: Transmission loss for an aluminium layer of thickness 5 mm (properties mentioned in Table 1) under plane wave excitation with  $\theta = 60^\circ$ . It is seen that thin plate theory is adequate to compute the vibro-acoustic indicators as both limiting frequencies ( $f_{\text{thin/thick}}$  &  $f_{\text{plate/solid}_{\text{df}}}$ ) are in the high frequencies.

435 For the plasterboard of 12.5 mm, it is seen from the Figs. 9 and 10 that  
 436 TL computed from thin plate theory is beginning to deviate from the elasticity  
 437 theory computation whereas thick plate theory is still in good agreement with  
 438 the elasticity theory until the limiting frequency  $f_{\text{plate/solid}_{\text{df}}}$ . This explains  
 439 the need to include the effect of shear into the anti-symmetric motion via  
 440 thick plate theory. Therefore, for these kind of materials, thick plate theory  
 441 would be appropriate to compute the acoustic indicators.

443 In case of a concrete layer with 140 mm thickness, it is noted from Figs. 11  
 444 and 12 that a similar trend is observed as for the plasterboard, that is, thin

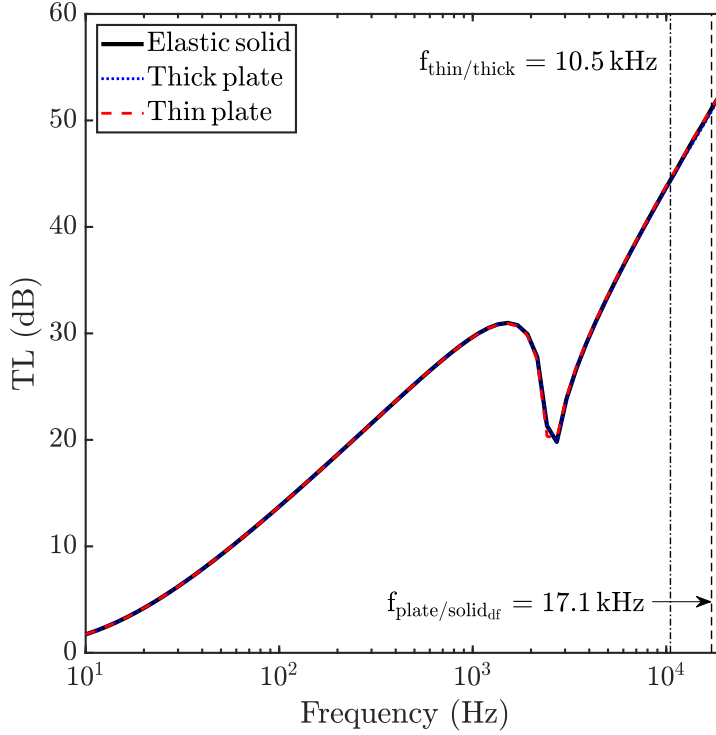


Figure 8: Transmission loss for an aluminium layer of thickness 5 mm (properties mentioned in Table 1) under diffuse field excitation. It is seen that thin plate theory is adequate to compute the vibro-acoustic indicators as both limiting frequencies ( $f_{\text{thin/thick}}$  &  $f_{\text{plate/solid}_{\text{df}}}$ ) are in the high frequencies.

445 and thick plate theories are starting to deviate from the elasticity theory  
446 computation at frequencies above  $f_{\text{thin/thick}}$  and  $f_{\text{plate/solid}_{\text{df}}}$ , respectively. One  
447 might also observe two notable points from the TL plots of concrete and plas-  
448 terboard. First, the coincidence frequency occurs after the limit frequency  
449 of thin plate ( $f_{\text{thin/thick}}$ ) in plasterboard whereas it can be spotted before  
450  $f_{\text{thin/thick}}$  in concrete. This implies that even for thicker material the thin  
451 plate theory might be still valid after the coincidence frequency. The sec-  
452 ond notable point is that the symmetric motion (or compressional motion)  
453 effect clearly appears in concrete. In Fig. 12, the second minima in the TL  
454 computed from the theory of elasticity corresponds to the compressional fre-  
455 quency ( $f_{\text{comp}} \approx 15$  kHz) given by Eq. (17). Therefore, it is inferred that the  
456 compressional mode can still be neglected for plasterboard whereas it has to  
457 be taken into account for the concrete layer and this is possible via employing  
458 the theory of elasticity. The same is observed from the TL plots (Figs. 13

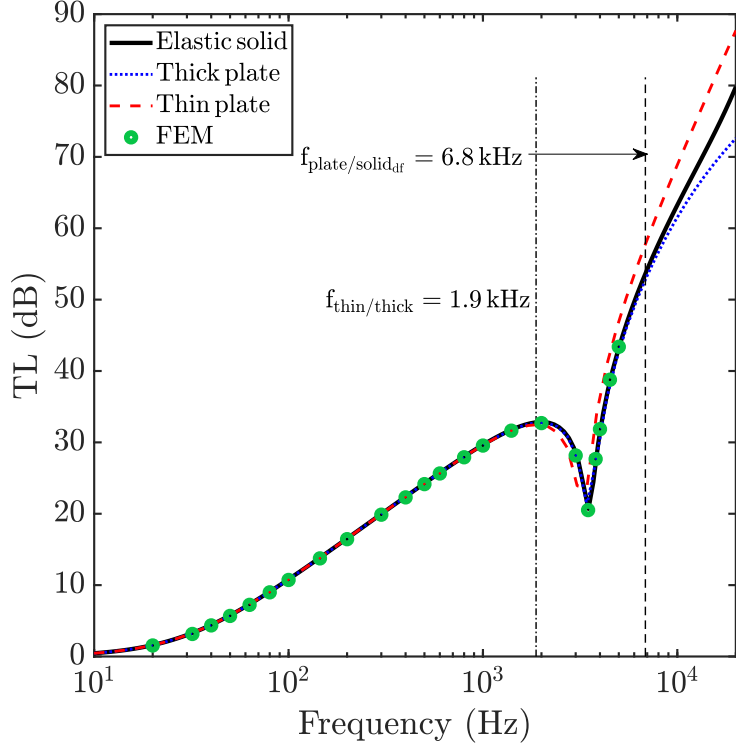


Figure 9: Transmission loss for a plasterboard layer of thickness 12.5 mm (properties mentioned in Table 1) under plane wave excitation with  $\theta = 60^\circ$ . Deviations of thin and thick plate theories from the elastic solid theory (or FEM) are observed after  $f_{\text{thin/thick}}$  and  $f_{\text{plate/solid}_{df}}$  respectively.

459 & 14) of soft layer with 20 mm thickness. It can be seen that TL of soft  
 460 layer is greatly influenced by the symmetric motion after the frequency limit  
 461  $f_{\text{plate/solid}_{df}}$ .

462 One can also observe from Eq. (20) that, for different materials of in-  
 463 finitely extending layers with same thickness, the frequency limit  $f_{\text{thin/thick}}$   
 464 would result in different values despite thicknesses being the same. Therefore,  
 465 it can be inferred that the use of thin plate theory requires proper combina-  
 466 tion of thickness and material properties (as given by Eq. (20)) rather than  
 467 comparing the thickness to the lateral dimensions. Similar argument holds  
 468 for  $f_{\text{plate/solid}_{df}}$  as well. In the previous TL plots, the choice of the values of  
 469  $C_k = 4$  and  $C_y = 10$  are further confirmed by the TL variation of plate theo-  
 470 ries from the elasticity theory and the TL difference between the elasticity  
 471 theory and plate theories are observed to be below 1 dB at the frequency  
 472 limits. Of course, one can conveniently choose the appropriate value of  $C_k$

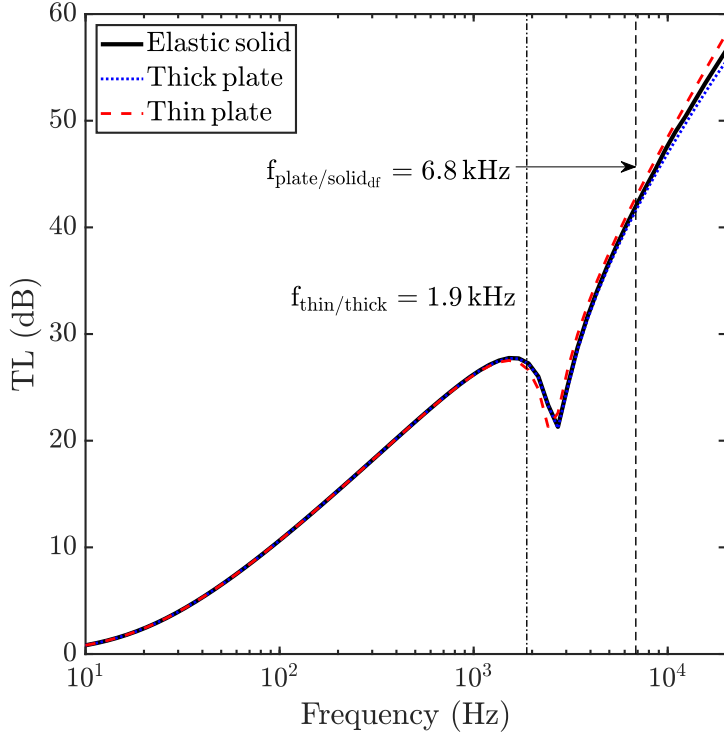


Figure 10: Transmission loss for a plasterboard layer of thickness 12.5 mm (properties mentioned in Table 1) under diffuse field excitation. Deviations of thin and thick plate theories from the elastic solid theory are observed after  $f_{\text{thin/thick}}$  and  $f_{\text{plate/solid}_{\text{df}}}$  respectively.

473 and  $C_y$  based on the tolerance accepted for the particular acoustic design.

#### 474 5.1. Further observation

475 In the case of finite sized plates, generally, the acoustic indicators com-  
476 puted from the infinitely extent layer theories would yield some discrepancies  
477 in the low to mid frequencies compared with experimental tests. Therefore,  
478 there are some works in the literature [5, 50] which focus on correcting the  
479 acoustic indicators by introducing correction factors that account for geo-  
480 metrical size effect. Since the radiation efficiency (which accounts for size  
481 correction in sound transmission problems) is reaching unity near the criti-  
482 cal frequency of the plate [44], the effects due to finite size is mainly visible  
483 at low frequencies below the critical frequency. Since the frequency limits  
484 ( $f_{\text{thin/thick}}$  and  $f_{\text{plate/solid}_{\text{df}}}$ ) of typical industrial materials fall near and/or af-  
485 ter the critical frequency, these limiting expressions obtained from infinite

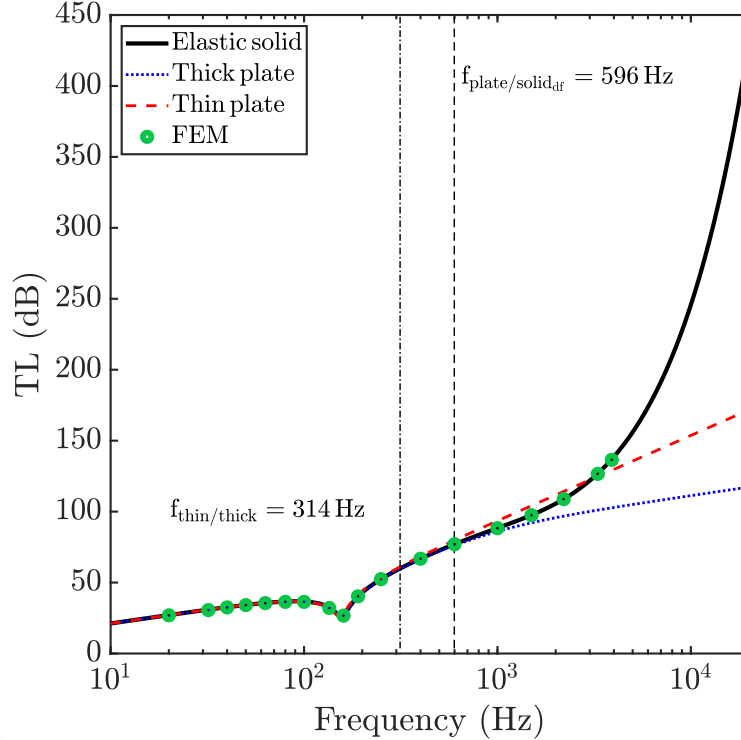


Figure 11: Transmission loss for a concrete layer of thickness 140 mm (properties mentioned in Table 1) under plane wave excitation with  $\theta = 60^\circ$ . Deviations of thin and thick plate theories from the elastic solid theory (or FEM) start to appear after  $f_{\text{thin/thick}}$  and  $f_{\text{plate/solid}_{\text{df}}}$  respectively.

486 plate theories are applicable to the finite size plate as well. For example,  
 487 this can be observed from the transmission loss computed from the finite size  
 488 correction model by Rhazi and Atalla [50] for the plasterboard of 12.5 mm  
 489 thickness under diffuse field excitation in Fig 15.

## 490 6. Concluding remarks

491 The assumptions used in thin and thick plate theories limit their applica-  
 492 bility in commonly used industrial materials after a certain frequency. Thin  
 493 plate theory attains the limitation since it does not account for the shear  
 494 effect in the anti-symmetric motion of the plate whereas this is considered in  
 495 thick plate theories. Nevertheless, both types of plate theories are approxi-  
 496 mations since they neglect symmetric motion of the panel in their theoretical  
 497 formulation. By analysing the wavenumbers and admittances of the investi-

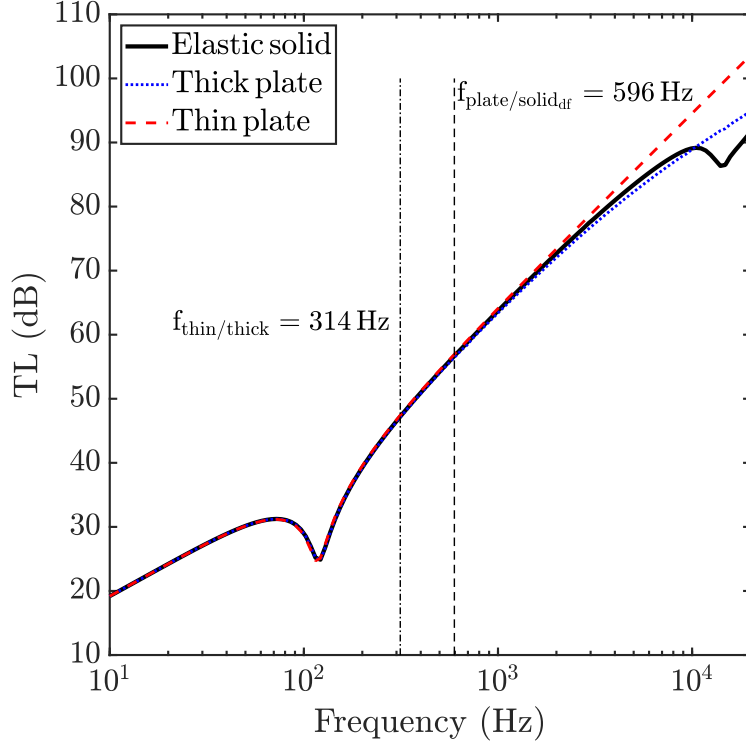


Figure 12: Transmission loss for a concrete layer of thickness 140 mm (properties mentioned in Table 1) under diffuse field excitation. Deviations of thin and thick plate theories from the elastic solid theory start to appear after  $f_{\text{thin/thick}}$  and  $f_{\text{plate/solid,df}}$  respectively.

498 gated structures, two frequency limits were presented in this manuscript: 1)  
 499 from the wave propagation analysis of the thick plate model, based on the  
 500 Reissner-Mindlin plate hypothesis, the analytical expression for the limiting  
 501 frequency of the thin plate model is derived, while 2) from comparing the  
 502 symmetric and anti-symmetric admittances, an analytical expression for the  
 503 limiting frequency of plate theories is derived. These two simple analytical  
 504 expressions for computing the limit of thin and thick plate theories can be  
 505 useful to choose the appropriate model in each case. Deviations of the TL  
 506 predictions obtained from different models are observed above these two lim-  
 507 iting frequencies. It is also shown that, although the limiting expressions  
 508 are derived from infinite layer theories, they can be applied to finite sized  
 509 layers as well. Due to the omission of shear effects in thin plate theories,  
 510 the refined coincidence and critical frequencies are derived from thick plate  
 511 theories. Finally, it is observed that plate theories quickly fail for materials  
 512 that are too soft in terms of longitudinal compression.

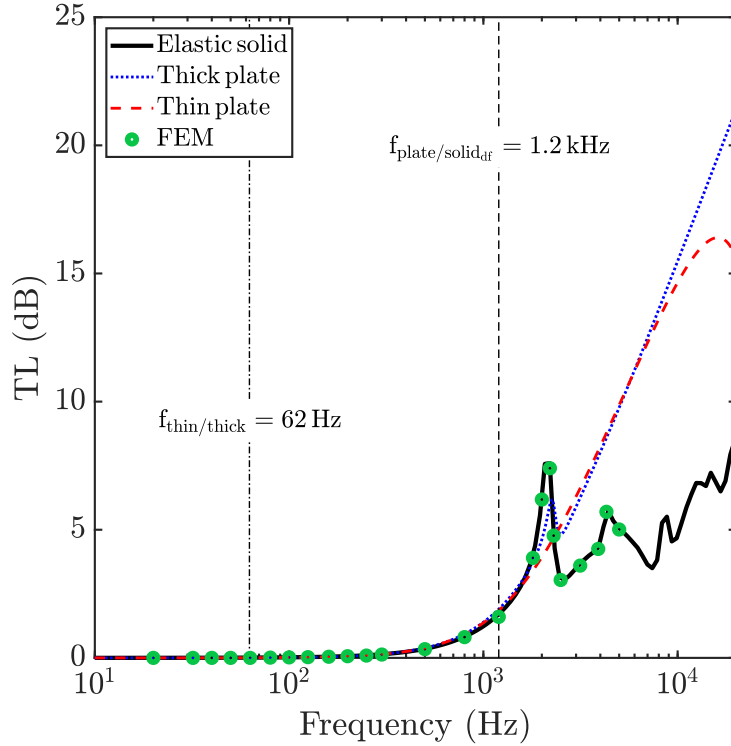


Figure 13: Transmission loss for a soft layer of thickness 20 mm (properties mentioned in Table 1) under plane wave excitation with  $\theta = 60^\circ$ . Deviations of plate theories from the elastic solid theory (or FEM) start to appear after  $f_{\text{plate/solid,df}}$ .

### 513 Acknowledgments

514 The authors would like to gratefully acknowledge Marie-Sklodowska Curie  
 515 Actions (MSCA) Project 765472 ‘N2N: No2Noise’ for the financial support.

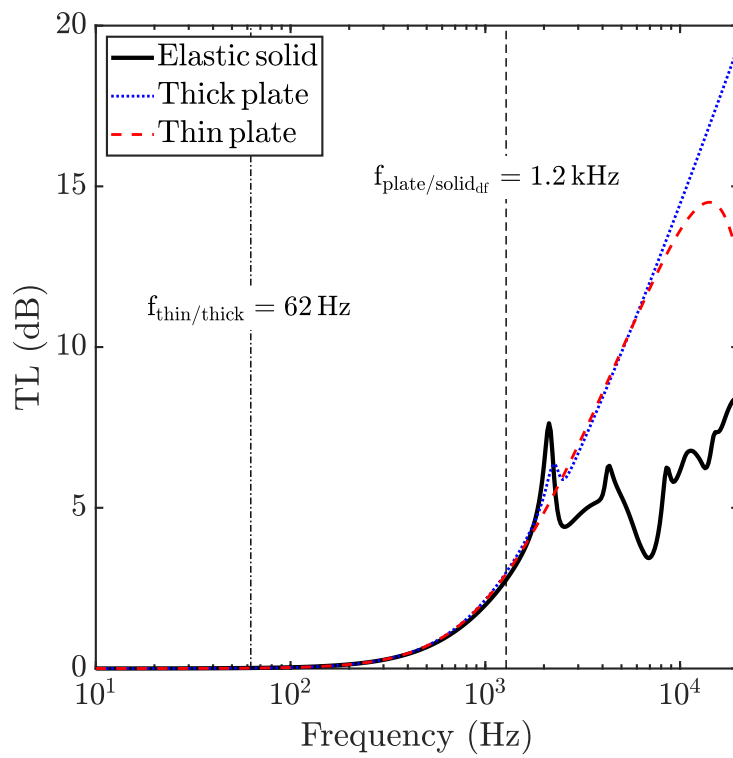


Figure 14: Transmission loss for a soft layer of thickness 20 mm (properties mentioned in Table 1) under diffuse field excitation. Deviations of plate theories from the elastic solid theory start to appear after  $f_{\text{plate/solid}_{\text{df}}}$ .

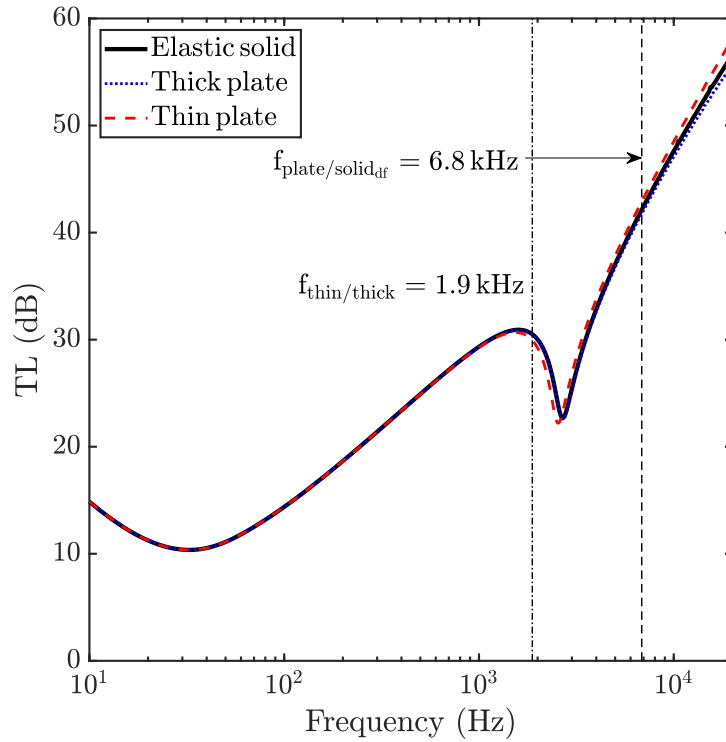


Figure 15: Transmission loss, computed from spatial windowing method by Rhazi and Atalla [50], across a finite size ( $3 \text{ m} \times 4 \text{ m}$ ) plasterboard of thickness 12.5 mm (properties are mentioned in Table 1) under diffuse field excitation. It is observed that limiting frequencies computed for infinite plate are still valid for the finite plates as the size correction effects minimal near the critical frequency of the plate.

516 **Appendix A. The transfer matrix of an elastic isotropic solid**

The transfer matrix of an elastic isotropic layer (defined by the equation  $V^{ES}(M) = [T^{ES}]_{4 \times 4} V^{ES}(M')$  where  $V^{ES} = \{u, v, \sigma_{zz}, \sigma_{xz}\}^T$ ) based on elasticity theory can be written as follows:

$$[T^{ES}]_{4 \times 4} = \frac{1}{D_1 + D_2 k_t} [T_{pq}^{ES}] \quad \text{where } p, q = 1 \text{ to } 4.$$

517 The matrix elements ( $T_{pq}^{ES}$ ) are,

518  $T_{11} = T_{44} = D_1 \cos(hk_{sz}) + D_2 k_t \cos(hk_{lz}),$

519  $T_{22} = T_{33} = D_1 \cos(hk_{lz}) + D_2 k_t \cos(hk_{sz}),$

520  $T_{12} = T_{34} = -j[D_2 k_{lz} k_{sz} \sin(hk_{sz}) - D_1 k_t \sin(hk_{lz})]/k_{lz},$

521  $T_{21} = T_{43} = j[D_2 k_{sz} k_{lz} \sin(hk_{lz}) - D_1 k_t \sin(hk_{sz})]/k_{sz},$

522  $T_{13} = T_{24} = \omega k_t [\cos(hk_{sz}) - \cos(hk_{lz})],$

523  $T_{31} = T_{42} = \left( \frac{D_1 D_2}{\omega^2 k_t} \right) T_{13},$

524  $T_{14} = -j\omega [k_{lz} k_{sz} \sin(hk_{sz}) + k_t^2 \sin(hk_{lz})]/k_{lz},$

525  $T_{23} = -j\omega [k_{lz} k_{sz} \sin(hk_{lz}) + k_t^2 \sin(hk_{sz})]/k_{sz},$

526  $T_{32} = -j[D_2^2 k_{lz} k_{sz} \sin(hk_{sz}) + D_1^2 \sin(hk_{lz})]/(\omega k_{lz}),$

527  $T_{41} = -j[D_2^2 k_{lz} k_{sz} \sin(hk_{lz}) + D_1^2 \sin(hk_{sz})]/(\omega k_{sz}),$

528 where  $D_1 = \mu(k_{sz}^2 - k_t^2)$  and  $D_2 = 2\mu k_t$ .

529 **References**

- 530 [1] L. Cremer, Theorie der schalldämmung dünner wände bei schrägem  
531 einfall [theory of sound insulation for oblique incidence], *Akustische*  
532 *Zeitschrift* 7 (1942) 81–104.
- 533 [2] M. Crocker, A. Price, Sound transmission using statistical energy anal-  
534 ysis, *Journal of Sound and Vibration* 9 (1969) 469–486.
- 535 [3] E. Sewell, Transmission of reverberant sound through a single-leaf par-  
536 tition surrounded by an infinite rigid baffle, *Journal of Sound and Vi-*  
537 *bration* 12 (1970) 21–32.
- 538 [4] F. G. Leppington, K. Heron, E. G. Broadbent, S. M. Mead, Resonant  
539 and non-resonant acoustic properties of elastic panels. II. The transmis-  
540 sion problem, *Proceedings of the Royal Society of London. A. Mathe-*  
541 *matical and Physical Sciences* 412 (1987) 309–337.
- 542 [5] M. Villot, C. Guigou, L. Gagliardini, Predicting the acoustical radiation  
543 of finite size multi-layered structures by applying spatial windowing on  
544 infinite structures, *Journal of Sound and Vibration* 245 (2001) 433–455.
- 545 [6] S. Ljunggren, A new type of solution for plate vibrations at low fre-  
546 quencies, *Journal of Sound and Vibration* 116 (1987) 125–136.
- 547 [7] A. E. H. Love, XVI. The small free vibrations and deformation of a  
548 thin elastic shell, *Philosophical Transactions of the Royal Society of*  
549 *London.(A.)* (1888) 491–546.
- 550 [8] J. L. Davy, Predicting the sound insulation of single leaf walls: Extension  
551 of Cremer’s model, *The Journal of the Acoustical Society of America*  
552 126 (2009) 1871–1877.
- 553 [9] M. Heckl, U. Donner, Schalldämmung dicker Wände (Sound insulation  
554 of thick walls), *Rundfunktech Mitt* 29 (1985) 287–291.
- 555 [10] R. Mindlin, Influence of rotary inertia and shear on flexural motions of  
556 isotropic elastic plates, *ASME Journal of Applied Mechanics* 18 (1951).
- 557 [11] E. Reissner, The effect of transverse shear deformation on the bending of  
558 elastic plates, *ASME Journal of Applied Mechanics* 12 (1945) A69–A77.
- 559 [12] H. Hencky, über die Berücksichtigung der Schubverzerrung in ebenen  
560 Platten [on the introduction of shear motion in flat plates], *ingenieur-*  
561 *archiv* 16 (1947) 72–76.

- 562 [13] S. Ljunggren, Airborne sound insulation of thick walls, *The Journal of*  
563 *the Acoustical Society of America* 89 (1991) 2338–2345.
- 564 [14] S. Ljunggren, Forced vibrations of infinite plates, *Journal of Sound and*  
565 *Vibration* 121 (1988) 221–236.
- 566 [15] E. Carrera, An assessment of mixed and classical theories on global and  
567 local response of multilayered orthotropic plates, *Composite Structures*  
568 50 (2000) 183–198.
- 569 [16] E. Carrera, Theories and finite elements for multilayered, anisotropic,  
570 composite plates and shells, *Archives of Computational Methods in*  
571 *Engineering* 9 (2002) 87–140.
- 572 [17] M. Levinson, An accurate, simple theory of the statics and dynamics of  
573 elastic plates, *Mechanics Research Communications* 7 (1980) 343–350.
- 574 [18] J. N. Reddy, A simple higher-order theory for laminated composite  
575 plates, *Journal of Applied Mechanics* 51 (1984) 745–752.
- 576 [19] M. Touratier, An efficient standard plate theory, *International Journal*  
577 *of Engineering Science* 29 (1991) 901–916.
- 578 [20] M. Karama, K. Afaq, S. Mistou, Mechanical behaviour of laminated  
579 composite beam by the new multi-layered laminated composite struc-  
580 tures model with transverse shear stress continuity, *International Jour-*  
581 *nal of Solids and Structures* 40 (2003) 1525–1546.
- 582 [21] X. Lu, D. Liu, Interlayer shear slip theory for cross-ply laminates with  
583 nonrigid interfaces, *AIAA Journal* 30 (1992) 1063–1073.
- 584 [22] C.-T. Sun, J. Whitney, Theories for the dynamic response of laminated  
585 plates, *AIAA Journal* 11 (1973) 178–183.
- 586 [23] R. Ford, P. Lord, A. Walker, Sound transmission through sandwich  
587 constructions, *Journal of Sound and Vibration* 5 (1967) 9–21.
- 588 [24] C. Smolenski, E. Krokosky, Dilational-mode sound transmission in sand-  
589 wich panels, *The Journal of the Acoustical Society of America* 54 (1973)  
590 1449–1457.
- 591 [25] J. Moore, R. Lyon, Sound transmission loss characteristics of sandwich  
592 panel constructions, *The Journal of the Acoustical Society of America*  
593 89 (1991) 777–791.

- 594 [26] S. Narayanan, R. Shanbhag, Sound transmission through a damped  
595 sandwich panel, *Journal of Sound and Vibration* 80 (1982) 315–327.
- 596 [27] S. Ghinet, N. Atalla, Modeling thick composite laminate and sandwich  
597 structures with linear viscoelastic damping, *Computers & Structures* 89  
598 (2011) 1547–1561.
- 599 [28] S. Srinivas, A refined analysis of composite laminates, *Journal of Sound*  
600 *and Vibration* 30 (1973) 495–507.
- 601 [29] J.-L. Guyader, C. Lesueur, Acoustic transmission through orthotropic  
602 multilayered plates, Part I: Plate vibration modes, *Journal of Sound*  
603 *and Vibration* 58 (1978) 51–68.
- 604 [30] J.-L. Guyader, C. Lesueur, Acoustic transmission through orthotropic  
605 multilayered plates, part II: Transmission loss, *Journal of Sound and*  
606 *Vibration* 58 (1978) 69–86.
- 607 [31] C. Lee, D. Liu, Layer reduction technique for composite laminate anal-  
608 ysis, *Computers & Structures* 44 (1992) 1305–1315.
- 609 [32] R. L. Woodcock, Free vibration of advanced anisotropic multilayered  
610 composites with arbitrary boundary conditions, *Journal of Sound and*  
611 *Vibration* 312 (2008) 769–788.
- 612 [33] A. Loredo, A. Castel, A multilayer anisotropic plate model with warp-  
613 ing functions for the study of vibrations reformulated from Woodcock’s  
614 work, *Journal of Sound and Vibration* 332 (2013) 102–125.
- 615 [34] A. Loredo, A multilayered plate theory with transverse shear and normal  
616 warping functions, *Composite Structures* 156 (2016) 361–374.
- 617 [35] D. Ross, Damping of plate flexural vibrations by means of viscoelastic  
618 laminae, *Structural Damping* (1959) 49–97.
- 619 [36] E. M. Kerwin Jr, Damping of flexural waves by a constrained viscoelastic  
620 layer, *The Journal of the Acoustical Society of America* 31 (1959) 952–  
621 962.
- 622 [37] E. E. Ungar, E. M. Kerwin Jr, Loss factors of viscoelastic systems  
623 in terms of energy concepts, *The Journal of the Acoustical Society of*  
624 *America* 34 (1962) 954–957.

- 625 [38] J.-L. Guyader, C. Cacciolati, Viscoelastic properties of single layer plate  
626 material equivalent to multi-layer composites plate, in: Turkish Acous-  
627 tical Society - 36th International Congress and Exhibition on Noise Con-  
628 trol Engineering, Inter-Noise 2007 Istanbul, volume 3, 2007, pp. 1558–  
629 1567.
- 630 [39] F. Marchetti, K. Ege, Q. Leclere, N. Roozen, On the structural dy-  
631 namics of laminated composite plates and sandwich structures; a new  
632 perspective on damping identification, *Journal of Sound and Vibration*  
633 474 (2020) 115256.
- 634 [40] Ö. Civalek, Harmonic differential quadrature-finite differences coupled  
635 approaches for geometrically nonlinear static and dynamic analysis of  
636 rectangular plates on elastic foundation, *Journal of Sound and Vibration*  
637 294 (2006) 966–980.
- 638 [41] K. Bhaskar, T. Varadan, *Plates: theories and applications*, John Wiley  
639 & Sons, 2014.
- 640 [42] J. Allard, N. Atalla, *Propagation of Sound in Porous Media: Modelling*  
641 *Sound Absorbing Materials 2e*, John Wiley & Sons, 2009.
- 642 [43] G. Kirchhoff, Über Das Gleichgewicht Und Die Bewegung Einer Elastis-  
643 chen Scheibe [On the balance and movement of an elastic disc], 1850.
- 644 [44] L. Cremer, M. Heckl, *Structure-Borne Sound: Structural Vibrations*  
645 *and Sound Radiation at Audio Frequencies*, Springer Science & Business  
646 Media, 2013.
- 647 [45] E. Magrab, *Vibrations of elastic structural members*, Alphen aan den  
648 Rijn, Sijthoff and Noordhoff (1979).
- 649 [46] J.-M. Berthelot, F. F. Ling, *Composite Materials: Mechanical Behavior*  
650 *and Structural Analysis*, Springer, 1999.
- 651 [47] D. Folds, C. Loggins, Transmission and reflection of ultrasonic waves  
652 in layered media, *The Journal of the Acoustical Society of America* 62  
653 (1977) 1102–1109.
- 654 [48] C. L. Dym, M. A. Lang, Transmission of sound through sandwich panels,  
655 *The Journal of the Acoustical Society of America* 56 (1974) 1523–1532.
- 656 [49] C. L. Dym, C. S. Ventres, M. A. Lang, Transmission of sound through  
657 sandwich panels: a reconsideration, *The journal of the acoustical society*  
658 *of America* 59 (1976) 364–367.

659 [50] D. Rhazi, N. Atalla, A simple method to account for size effects in  
660 the transfer matrix method, *The Journal of the Acoustical Society of*  
661 *America* 127 (2010) EL30–EL36.